JOURNAL OF Materials CHEMISTRY

Solid–gas interaction of nitrogen oxide adsorbed on MnO_x–CeO_2: a DRIFTS study†

Masato Machida,* Masatoshi Uto, Daisuke Kurogi and Tsuyoshi Kijima

Department of Applied Chemistry, Faculty of Engineering, Miyazaki University, 1-1 Gakuenkibanadai Nishi, Miyazaki 889-2192, Japan. E-mail: t0g101u@cc.miyazaki-u.ac.jp; Fax: +81-985-58-7323

Received 18th September 2000, Accepted 1st November 2000
First published as an Advance Article on the web 26th January 2001

The formation of fluorite-type solid solutions with compositions $(n)MnO_x$–$(1-n)CeO_2$ is effective in increasing adsorptive NO uptake. Solid–gas interactions for NO adsorbed onto preoxidized samples was studied by the use of diffuse reflectance Fourier transform infrared spectroscopy (DRIFTS) to elucidate the role of each oxide component. On exposure to a flowing gas containing 0.04% NO, several different types of nitrate and/or nitrite were yielded depending on temperature (25 and 150 °C), O_2 concentration (0, 2, and 10%) in the gas feed, and composition of the binary oxide ($n=0$, 0.25, 0.5, and 1.0). On CeO_2 ($n=0$), chelating nitrite (NO_2^-) prevailed, while only small amounts of bidentate and unidentate nitrates (NO_3^-) were formed at 150 °C. By contrast, adsorption onto MnO_x ($n=1.0$) at 150 °C produced bidentate nitrate even in the absence of O_2, suggesting that the lattice oxygen takes part in the NO oxidation process. On MnO_x–CeO_2 ($n=0.25$ and 0.5), chelating nitrite bound to Ce ions was increasingly converted to nitrate at higher O_2 concentration and at elevated temperature. A surface reaction model on the basis of the DRIFTS results reveals that the redox of Mn ions with simultaneous oxygen equilibration with the gas phase should play a key role in facilitating the oxidative adsorption of NO.

Introduction

A number of metal oxides are known to exhibit high reactivity toward gaseous NO, which results in adsorption, absorption or solid–gas reactions at relatively low temperature (<200 °C).[1,2] For instance, metal oxides containing alkaline or alkaline-earth elements, such as K and Ba, bring about NO adsorption as nitrate (NO_3^-) in the presence of O_2 or nitrite (NO_2^-) even in the absence of O_2. The high reactivity is associated with the strong basicity of the lattice oxide ions surrounding these alkaline cations. The reported NO_x-sorbing materials based on this type include Ba–Y–Cu–O,[3] Ba–Cu–O,[4,5] La–Ba–Sr–Cu–O,[6–9] Ba–Al_2O_3,[10] and $BaSnO_3$.[11] For these materials, one serious obstacle to practical application is that NO adsorption is significantly inhibited by CO_2, because CO_2 and NO_x are competing for basic sites on the solid surface.[1] Another possible way to design efficient NO_x sorbents is by combination of NO oxidation catalysts and NO_2-sorbing components.[1] On such solids, gaseous NO is oxidized to NO_2 and subsequently sorbed as nitrite or nitrate ions even at ambient temperature. NO_x sorbents based on this concept include MnO_2–ZrO_2,[12,13] MnO_x–CeO_2,[14,15] Pt/ZrO_2–Al_2O_3,[16] and Pd/ZrO_2.[17] We have previously reported the NO_x-sorbing property of MnO_x–CeO_2 binary oxides and their use as support materials for low-temperature NO_x reduction in a strongly oxidizing atmosphere.[14,15] The NO_x uptake, which was increased by decreasing the reaction temperature and/or by increasing the O_2 concentration in the gas feed, suggests chemisorption *via* oxidation of NO. A large NO uptake is therefore considered to be associated with the combination of the NO-oxidation activity of MnO_x and the NO_x-adsorption ability of CeO_2, which should possibly yield noticeable synergism in the oxidative adsorption. However, further understanding of the surface reaction mechanism requires spectroscopic evidence for the adsorption species formed on binary oxides with different compositions under various reaction conditions.

In the present work, we have employed DRIFTS to study the structure of NO adsorbed species and their changes caused by variations in the temperature and O_2 concentration in the gas feed over MnO_x–CeO_2 solid solutions with different compositions. The results were correlated with the amount of NO uptake to elucidate the role of manganese in the oxidative NO adsorption.

Experimental

Sample preparation and characterization

Precursors of the binary oxides, $(n)MnO_x$–$(1-n)CeO_2$, were prepared by coprecipitation from aqueous solutions of nitrates at ambient temperature. Calculated amounts of $Mn(NO_3)_2{\cdot}6H_2O$ and $Ce(NO_3)_3{\cdot}6H_2O$ (Wako Chemicals, guaranteed reagent grade) were dissolved in distilled deionized water. An aqueous solution of ammonia was added dropwise to the solution under vigorous stirring. The resultant light-brown suspension obtained with a final pH of 12 was evaporated to dryness and subsequently calcined at 450 °C or 800 °C for 5 h in air. XRD patterns of as-calcined powder samples were obtained using by a Shimadzu XD-D1 diffractometer with a monochromated CuK_α radiation source (30 kV, 30 mA). BET surface area values were obtained by measuring N_2 adsorption isotherms at −196 °C.

NO adsorption

Adsorptive removal of NO_x was measured in a conventional flow reactor, which consisted of mass flow controllers, valves, gas mixers, stainless tubes and an infrared image furnace. The granular sample (10–20 mesh, 0.2 g) was fixed in a quartz tube (4 mm i.d.) by packing quartz wool at both ends of the bed. Prior to the reaction, the sample was heated at 400 °C in a

† Presented at Solid State Chemistry 2000, Prague, Czech Republic, 4–8 September 2000.

 DOI: 10.1039/b007533g

stream of 20% O_2–He for 30 min. After cooling to 30 or 150 °C and subsequent purging with He, gaseous mixtures of 0.08% NO, 0–10% O_2, and He balance were fed to the sample at 50 cm^3 min^{-1} (W/F = 0.24 g s cm^{-3}). The effluent gas was analyzed by on-line gas chromatography (GL Science Model 370) with a molecular sieve 5A column and a chemiluminescence NO_x analyzer (Shimadzu NOA305).

DRIFTS measurement

DRIFT spectroscopy was conducted on a Jasco 610 spectrometer and a temperature-controllable diffuse reflectance reaction cell (Jasco DR600A) with a KBr window which was connected to a gas supply system to allow measurement under controlled gas environments at atmospheric pressure and temperatures up to 800 °C. The sample was finely ground and placed in a crucible inside the cell to be exposed to a flowing gas mixture. The sample was first preheated *in situ* in flowing 20% O_2–He at 400 °C for 1 h prior to any experiment. This was followed by cooling to 25 or 150 °C, purging with He, and subsequent admission of gas mixtures of 0.04% NO, 0–10%O_2, and He balance at 50 cm^3 min^{-1} for 30 min. No gas-phase conversion of NO to NO_2 was detected in the absence of MnO_x–CeO_2. Immediately following this procedure, the cell was purged with He for 5 min and cooled to 25 °C, where a spectrum was recorded in a stream of He (50 cm^3 min^{-1}). At a resolution of 4 cm^{-1}, 512 scans were usually recorded. All spectra thus obtained were transformed into absorption spectra by the use of the Kubelka–Munk function and referenced to those taken just before NO admission.

Results and discussion

Crystal structure of MnO_x–CeO_2

Fig. 1 and 2 represent powder XRD patterns of $(n)MnO_x$–$(1-n)CeO_2$ ($0 \leqslant n \leqslant 1.0$) after calcination at 450 °C and 800 °C, respectively. The samples calcined at 450 °C, with the exception of MnO_x ($n = 1.0$), showed diffraction peaks only ascribable to a CeO_2 phase with the cubic fluorite structure. These peaks were significantly broadened with increasing n probably because of the lattice distortion. Heating at 800 °C resulted in considerable crystallization of the fluorite phase, as can be judged from the sharpened diffraction peaks, which was accompanied by an incremental precipitation of Mn_2O_3 at $x \geqslant 0.4$. For comparison, a physical mixture of Mn_2O_3/CeO_2

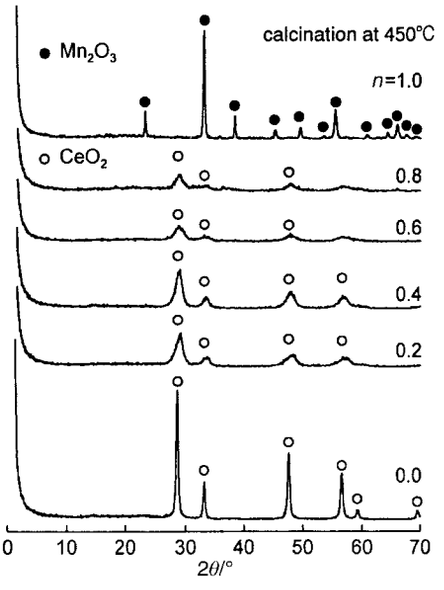

Fig. 1 Powder X-ray diffraction patterns of $(n)MnO_x$–$(1-n)CeO_2$ after calcination at 450 °C.

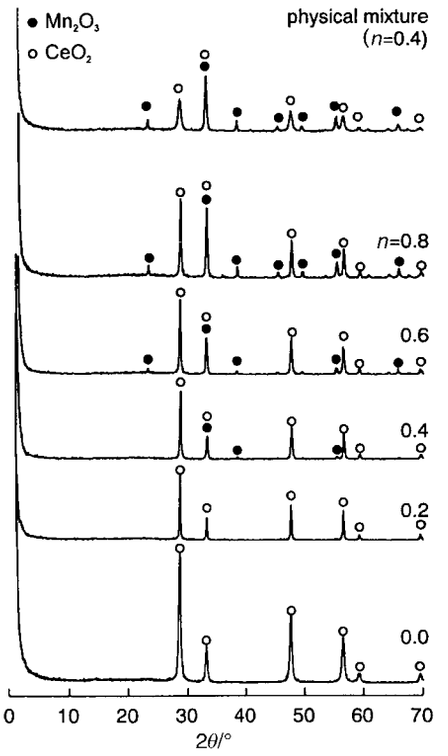

Fig. 2 Powder X-ray diffraction patterns of $(n)MnO_x$–$(1-n)CeO_2$ after calcination at 800 °C and a physical mixture of Mn_2O_3–CeO_2 powders with the composition of $n = 0.4$.

powders with a composition of $n = 0.4$ is shown at the top of Fig. 2. Clearly, the diffraction peaks from Mn_2O_3 for $n = 0.4$ are less intense compared to those in a corresponding physical mixture of Mn_2O_3–CeO_2 powders. These results support that a single phase of the fluorite-type solid solution was produced at least for $n \leqslant 0.2$. After calcination at 800 °C, the lattice parameter of the fluorite phase in the range $0.2 \leqslant n \leqslant 0.6$ is almost constant at 5.403 nm, compared to 0.5411 nm for CeO_2. Much more prominent dependence of the lattice parameter on the oxide composition was observed for the samples ($0 \leqslant n \leqslant 0.6$) calcined at 450 °C, which were supposedly composed of metastable pseudo-solid solutions. The decrease of the lattice parameter is associated with the small ionic radius of Mn^{3+} (0.66 nm) compared to Ce^{4+} (0.94 nm).[18] Generally, the formation of a substitutional solid solution is not favorable for systems having such a large difference of ionic radius. Nevertheless, the replacement of Ce^{4+} by Mn^{3+} in the fluorite structure seems to be possible when considering their structural similarity; the crystal structure of Mn_2O_3 is the C-rare earth type that is basically composed of anion-deficient units of fluorite structure.[19]

NO adsorption on MnO_x–CeO_2

The NO adsorption property of the present system is briefly described for the latter discussion. As was reported in our preceding paper,[14] the formation of the MnO_x–CeO_2 solid solution is significantly effective in not only accelerating NO adsorption, but also increasing the adsorptive capacity of NO at $\leqslant 200$ °C. Table 1 reports the BET surface area and NO uptake of $(n)MnO_x$–$(1-n)CeO_2$ after calcination at 450 °C. Here, the NO uptake is expressed in terms of mmol g^{-1} and molecule nm^{-2}, which mean molar quantity of adsorbed NO per unit weight and numbers of NO molecules adsorbed per unit surface area, respectively. An increase of the surface area is one of the reasons for the larger NO uptake per unit weight for $n = 0.25$. It also should be noted that the NO uptake also increased when calculated per unit surface area;

Table 1 NO uptake of $(n)MnO_x$–$(1-n)CeO_2$

		NO uptake/mmol g^{-1}				NO uptake/molecule nm^{-2a}			
n	Surface area/m^2 g^{-1}	25 °C	100 °C	150 °C	200 °C	25 °C	100 °C	150 °C	200 °C
0.00	64.5	0.084	0.069	0.074	0.049	0.78	0.64	0.69	0.46
0.25	80.1	0.196	0.139	0.119	0.130	1.47	1.04	0.89	0.98
0.50	64.2	0.170	0.105	0.092	0.101	1.59	0.98	0.86	0.95
0.75	54.7	0.142	0.086	0.086	0.083	1.56	0.95	0.95	0.91
1.00	14.8	0.033	0.032	0.035	0.032	1.34	1.30	1.42	1.30

[a]Calculated from NO uptake and surface area.

improved affinity of the solid surface toward NO contributes to the large NO uptake. On the other hand, the NO uptake per unit weight is smallest for $n=1.0$ (MnO_x) at 25–200 °C. This is largely due to the low specific surface area (14.8 m^2 g^{-1} after calcination at 450 °C); it is quite difficult to prepare large surface area manganese oxide with enough thermal stability. However, the highest NO uptake per unit surface area as shown in Table 1 clearly suggests that the surface of MnO_x exhibits the higher NO adsorbability, compared to pure CeO_2.

DRIFT study on NO_x adsorption

The different reactivity of the surface of $(n)MnO_x$–$(1-n)CeO_2$ toward NO was studied by the use of DRIFT spectroscopy. The spectra covering the range 700–4000 cm^{-1} were recorded at 25 °C after adsorption in the stream of 0.04% NO–He with different O_2 concentrations at 25 °C and 150 °C. All the spectra were referenced to that of the sample in flowing He just before exposure to NO. The assignments of absorption bands described below are consistent with those reported previously by several researchers.[20–24] The adsorbate species formed on the present system are classified as unidentate nitrate (NO_3^-, *ca.* 1460, 1300, and 1050 cm^{-1}), bidentate nitrate (NO_3^-, *ca.* 1630, 1550, 1050 cm^{-1}) and chelating nitrite (NO_2^-, *ca.* 1200 cm^{-1}). Other possible species including NO (*ca.* 1950 cm^{-1}), NO^- (1100–1170 cm^{-1}) and $N_2O_2^{2-}$ (1320–1370 cm^{-1}), which are reported to be observed over cerium oxide when outgassed at high temperatures,[24] were not resolved in our measurements, because these species are produced *via* reaction between NO and surface oxygen vacancies. In the present study, the preoxidation treatment at 400 °C in flowing O_2–He would minimize the formation of such surface vacancies on the samples.

As shown in Fig. 3a, exposure of MnO_x ($n=1.0$) to 0.04% NO–He at 25 °C produced two very weak bands at 1468 and 1325 cm^{-1}, which are attributed to asymmetric and symmetric NO_2 vibrations of unidentate nitrate (NO_3^-), respectively. These bands, which intensified with an increase of O_2 concentration, are consistent with more efficient conversion of NO to NO_3^- by the consumption of O_2 in the gas phase. When NO was introduced to MnO_x at 150 °C, a strong band at 1580 cm^{-1} typical of the asymmetric NO_2 vibration of bidentate nitrate was produced in the absence of O_2 (Fig. 3b). In this case, therefore, the lattice oxygen of MnO_x should be thermally activated to take part in the oxidation of NO. In addition to the band at 1580 cm^{-1}, bands ascribable to unidentate nitrate at 1440 and 1335 cm^{-1} became intense at higher O_2 concentrations. As was the case for adsorption at 25 °C, gaseous O_2 is required for NO oxidation to produce unidentate nitrate. The spectra taken at higher O_2 concentration showed a small negative peak at 1650–1700 cm^{-1}, which can be assigned to the loss of bidentate carbonates; these adsorbates, which probably originate from the adsorption of atmospheric CO_2, appear to be displaced by nitrate species.

The spectra observed for CeO_2 ($n=0$) were completely different from those obtained for MnO_x ($n=1.0$) as shown in Fig. 4. Adsorption in the absence of O_2 at 25 °C generated an intense band at 1203 cm^{-1} due to the symmetric NO_2 vibration of chelating nitrite (NO_2^-), the intensity of which was unchanged irrespective of the O_2 concentration. The broadening and asymmetric character of this peak is probably due to an overlap of peaks from the symmetric NO_2 vibration mode of unidentate nitrate (*ca.* 1300 cm^{-1}) and the N=O symmetric vibration mode of bidentate nitrate (1020–1050 cm^{-1}). In

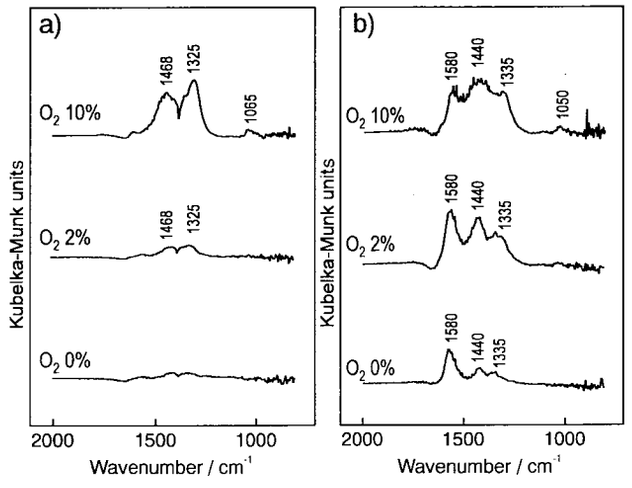

Fig. 3 DRIFT spectra of MnO_x ($n=1.0$) after NO adsorption at a) 25 °C and b) 150 °C. 0.04% NO, 0, 2, or 10% O_2, He balance, 50 cm^3 min^{-1}, 30 min.

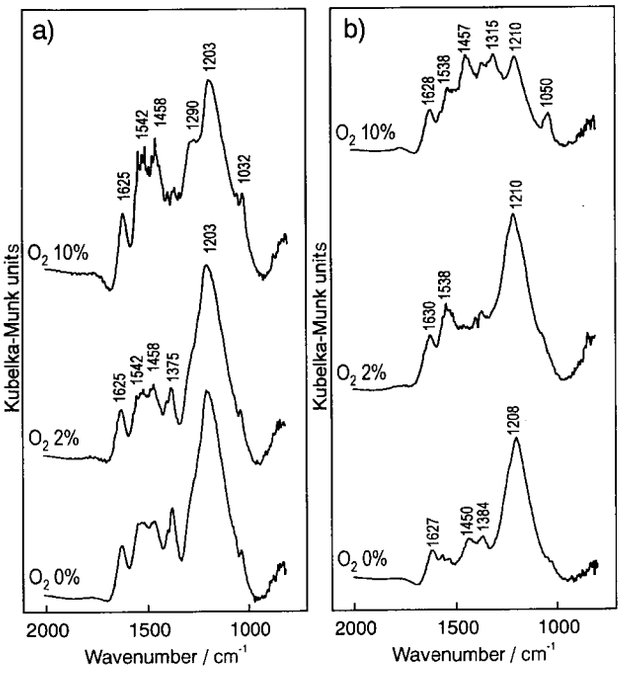

Fig. 4 DRIFT spectra of CeO_2 ($n=0$) after NO adsorption at a) 25 °C and b) 150 °C. 0.04% NO, 0, 2, or 10% O_2, He balance, 50 cm^3 min^{-1}, 30 min.

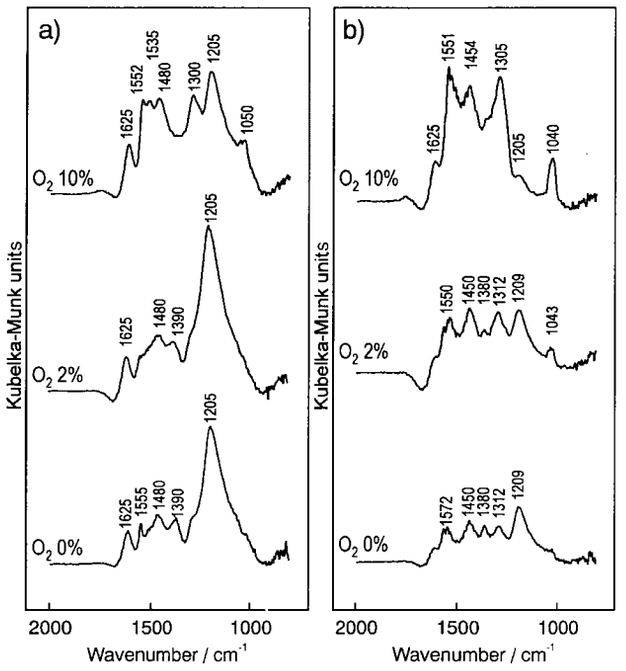

Fig. 5 DRIFT spectra of $0.25MnO_x$–$0.75CeO_2$ ($n=0.25$) after NO adsorption at a) 25 °C and b) 150 °C. 0.04% NO, 0, 2, or 10% O_2, He balance, 50 cm^3 min^{-1}, 30 min.

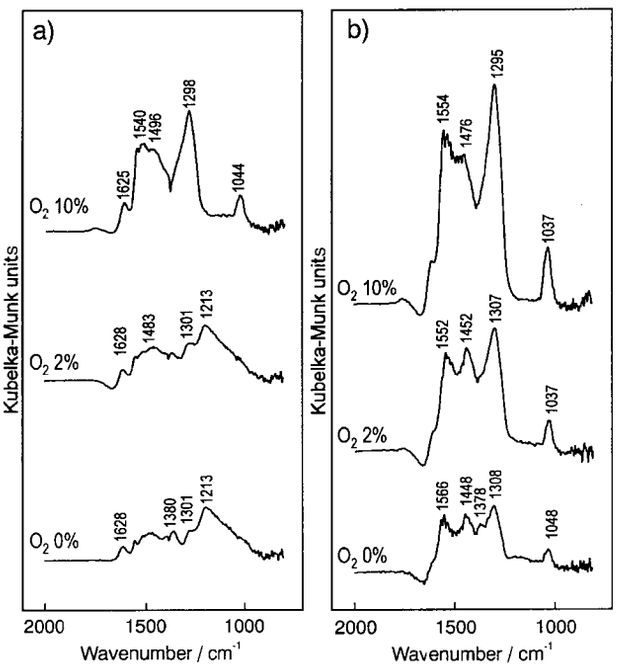

Fig. 6 DRIFT spectra of $0.5MnO_x$–$0.5CeO_2$ ($n=0.5$) after NO adsorption at a) 25 °C and b) 150 °C. 0.04% NO, 0, 2, or 10% O_2, He balance, 50 cm^3 min^{-1}, 30 min.

addition, complicated and ill-defined peaks from 1700 to 1350 cm^{-1} may be due to an overlap of nitrate (1625 and 1542 cm^{-1}) and unidentate nitrate bands (1458 cm^{-1}) and other unresolved bands. From the increased intensity of the nitrate bands at higher O_2 concentrations, oxidative adsorption of NO as NO_3^- takes place as in the MnO_x case. Unlike the MnO_x sample, however, a large part of chelating NO_3^- remained unchanged even at the highest O_2 concentration (10%). This is in accord with the lower NO oxidizing capability of CeO_2. More abundant nitrate species were observed when the adsorption was carried out at 150 °C in the presence of 10% O_2, where the chelating nitrite band (*ca.* 1210 cm^{-1}) diminished while bidentate and unidentate nitrate bands (1538, 1457, 1315, and 1050 cm^{-1}) developed.

Fig. 5 shows the result for $0.25MnO_x$–$0.75CeO_2$ ($n=0.25$), which shows the largest NO uptake per unit weight at 30–200 °C as shown in Table 1. The three spectra after adsorption at 25 °C were almost identical to those obtained for CeO_2 (Fig. 4a), *i.e.*, chelating nitrite is the dominant adsorbate in the absence of O_2, whereas incremental formation of bidentate/unidentate nitrates was observed at high O_2 concentrations. This is consistent with the formation of a homogeneous solid solution based on the CeO_2 fluorite structure, which possesses a surface composition nearly equal to the bulk composition.[14] At 150 °C, the nitrite band at 1209 cm^{-1} became much less intense and disappeared at 10% O_2 concentration, where the unidentate and bidentate nitrates are dominant species. From simple comparison of Fig. 4 with Fig. 5, it can be deduced that the oxidative NO adsorption from flowing gas mixtures is promoted as MnO_x is dissolved into the CeO_2 lattice. The effect of Mn on the NO oxidation was more clearly evidenced for $0.5MnO_x$–$0.5CeO_2$ ($n=0.5$) as shown in Fig. 6. Adsorption of NO at 25 °C created bands similar to those found for $0.25MnO_x$–$0.75CeO_2$, because the band at 1213 cm^{-1} (chelating nitrite) is strongest at lower O_2 concentration while bands at 1700–1300 cm^{-1} intensified at higher O_2 concentrations. At 10% O_2, a noticeable change was observed: formation of a strong and sharp band at *ca.* 1300 cm^{-1} due to the unidentate nitrate with simultaneous disappearance of the chelating nitrate band at *ca.* 1200 cm^{-1}. Facilitated conversion of nitrite to nitrate is more obvious at 150 °C (Fig. 6b); *i.e.*, exposure to NO in the absence of O_2 created no nitrite bands at 1200 cm^{-1} but strong nitrate bands between 1600 and 1300 cm^{-1} were produced. Since these nitrate bands were very weak over CeO_2 alone (Fig. 4b), new sites available for nitrate-type adsorption must be produced on the surface of MnO_x–CeO_2 solid solutions. The 1300 cm^{-1} band intensified with an increase of n in $(n)MnO_x$–$(1-n)CeO_2$, but the observed peak position was shifted from that observed over MnO_x (1325–1335 cm^{-1}).

Solid–gas interaction in oxidative adsorption

On the basis of the DRIFTS results, possible reaction schemes for the oxidative adsorption of NO onto $(n)MnO_x$–$(1-n)CeO_2$ can be derived as depicted in Fig. 7. On MnO_x, the adsorption of NO in the presence of O_2 creates unidentate NO_3^- at 25 °C (Fig. 7a), because the NO–O_2 reaction is efficiently catalyzed over Mn_2O_3. At 150 °C, NO can be oxidized directly by the lattice oxygen to form bidentate nitrate (Fig. 7b). Thus, the large NO uptake per unit surface area of the MnO_x (Table 1) is associated with the redox property of the surface. The adsorption onto CeO_2 also involves the reaction with lattice oxygen; NO reacts with a basic oxygen site adjacent to Ce^{4+} on the surface to produce chelating NO_2^-, which was never observed on MnO_x (Fig. 7c). Owing to the lack of oxidizing ability, however, the conversion of NO_2^- to NO_3^- is difficult to complete even in a strongly oxidizing atmosphere and at 150 °C. As shown in Fig. 7d, the MnO_x–CeO_2 solid solution produces chelating NO_2^- on the Ce site in a similar way (I), but the following oxidation to unidentate or bidentate NO_3^- (IV) was brought about by lattice oxygen bound to Mn ions (II). Although this step is accompanied by the reduction of substituted Mn ions, the reoxidation should be easily accomplished by oxygen equilibration with the gas phase (III), thus leading to successive oxidative NO adsorption processes. Such redox property caused by substituted Mn ions in the solid solution was also supported by the use of O_2-TPD measurement in our previous work.[14] Although oxygen evolution from CeO_2 was negligible in accord with the higher stability against reduction, MnO_x–CeO_2 produced large O_2 desorption at <600 °C, which could be compensated by the

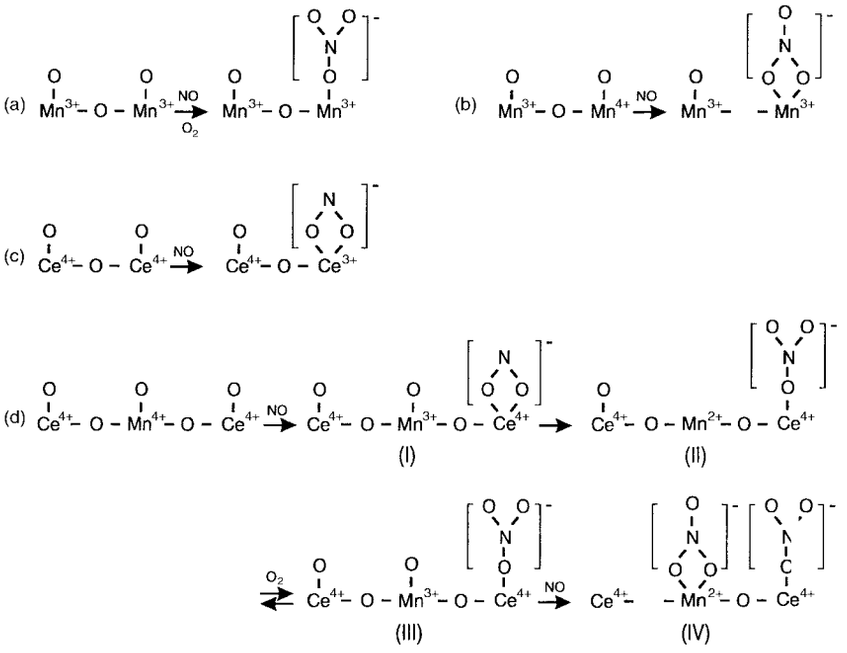

Fig. 7 Reaction schemes for oxidative NO adsorption onto CeO_2, MnO_x, and MnO_x–CeO_2.

reduction of Mn ions. At the present stage, we cannot define which of the cationic sites (Ce and Mn) is responsible for each of the adsorption species (bidentate/unidentate nitrates). By judging from similar spectra (Figs. 4 and 5), the adsorption over $0.25MnO_x$–$0.75CeO_2$ is considered to take place mainly on the Ce site. This is consistent with the higher basicity of Ce, so that the lattice oxygen bound to Ce appears to be more reactive toward NO compared to those bound to Mn. However, the adsorption at elevated temperature (150 °C) and high O_2 concentration produced very a large amount of unidentate nitrate (Fig. 6b), which may be formed on the Mn site exposed on the surface. The surface reaction model developed in this study represents the role of each component in the present MnO_x–CeO_2 solid solution. Manganese ions substituted into the CeO_2 lattice play the role of not only an efficient catalyst for NO oxidation in an oxidizing atmosphere, but also an oxidizing agent for NO when the O_2 partial pressure becomes low. On the other hand, Ce ions provide a number of adsorption sites on the surface, because the moderate basicity allows the surrounding oxide ions to react readily with the NO_x thus oxidized. These two different components occur as a pair site on the surface of the homogenous solid solution, resulting in noticeable synergism in the NO adsorbability. This is the reason why a large NO uptake is attained irrespective of the O_2 concentration in the gas feed, which is useful because such NO_x-sorbing materials can be applied for low temperature NO_x removal in a wide range of oxygen partial pressures.

Acknowledgement

The present study was partially supported by a Grant-in-Aid for Scientific Research from the Ministry of Education, Science, Sports, and Culture, Japan.

References

1 M. Machida, *Catalysis*, The Royal Society of Chemistry, Cambridge, 2000, vol. 15, p. 73.
2 H. Arai and M. Machida, *Catal. Today*, 1994, **22**, 97.
3 K. Tabata, H. Fukui, S. Kohiki, N. Mizuno and M. Misono, *Chem. Lett.*, 1988, 799.
4 M. Machida, K. Yasuoka, K. Eguchi and H. Arai, *J. Chem. Soc., Chem. Commun.*, 1990, 1165.
5 M. Machida, S. Ogata, K. Yasuoka, K. Eguchi and H. Arai, *Proc. Int. Congr. Catal.*, ed. L. Guczi, F. Solymosi and P. Tetenyi, Elsevier, Amsterdam, 1993, p. 2645.
6 M. Machida, H. Murakami and T. Kijima, *J. Mater. Chem.*, 1994, **4**, 1621.
7 M. Machida, H. Murakami, T. Kitsubayashi and T. Kijima, *Chem. Mater.*, 1996, **8**, 197.
8 M. Machida, H. Murakami, T. Kitsubayashi and T. Kijima, *Chem. Mater.*, 1997, **9**, 135.
9 M. Machida, H. Murakami, T. Kitsubayashi and T. Kijima, *Appl. Catal. B: Environ.*, 1996, **17**, 195.
10 S. Hodjati, P. Bernhardt, C. Petit, V. Pitchon and A. Kiennemann, *Appl. Catal. B: Environ.*, 1998, **19**, 209.
11 S. Hodjati, P. Bernhardt, C. Petit, V. Pitchon and A. Kiennemann, *Appl. Catal. B: Environ.*, 2000, **26**, 5.
12 K. Eguchi, M. Watabe, M. Machida and H. Arai, *Catal. Today*, 1996, **27**, 297.
13 K. Eguchi, M. Watabe, S. Ogata and H. Arai, *Bull. Chem. Soc. Jpn.*, 1995, **68**, 1739.
14 M. Machida, D. Kurogi and T. Kijima, *Chem. Mater.*, 2000, **12**, 3158.
15 M. Machida, D. Kurogi and T. Kijima, *Chem. Mater.*, 2000, **12**, 3165.
16 K. Eguchi and T. Hayashi, *Catal. Today*, 1998, **45**, 109.
17 M. Machida, A. Yoshii and T. Kijima, *Int. J. Inorg. Mater.*, 2000, **2**, 413.
18 *CRC Handbook of Chemistry and Physics*, ed. D. R. Lide, 72nd edn., CRC Press, Boston, 1991.
19 F. G. Galasso, *Structure and Properties of Inorganic Solids*, Pergamon, Oxford, 1970, p. 115.
20 K. Nakamoto, *Infrared and Raman Spectra of Inorganic and Coordination Compounds*, 4th edn., Wiley, New York, 1986.
21 B. Klingenberg and M. A. Vannice, *Appl. Catal. B: Environ.*, 1999, **21**, 19.
22 S. J. Huang, A. B. Walters and M. A. Vannice, *Appl. Catal. B: Environ.*, 2000, **26**, 101.
23 F. C. Meunier, V. Zuzaniuk, J. P. Breen, M. Olsson and J. R. H. Ross, *Catal. Today*, 2000, **59**, 287.
24 A. Martinez-Arias, J. Soria, J. C. Consesa, X. L. Seoane, A. Arcoya and R. Cataluna, *J. Chem. Soc., Faraday Trans.*, 1995, **91**, 1679.